Korean J. Chem. Eng., 33(4), 1170-1180 (2016)
DOI: 10.1007/s11814-015-0244-2

pISSN: 0256-1115
eISSN: 1975-7220

Ultrasonic method for measuring the gas holdup of gas-liquid bubbly flow in a small-diameter pipe

Zheng Gong, An Zhao, Lu-Sheng Zhai, Ying-Yu Ren, and Ning-De Jin†

School of Electrical Engineering and Automation, Tianjin University, Tianjin 300072, China
(*Received 24 June 2015 • accepted 17 November 2015*)

Abstract−Based on ultrasonic sound pressure attenuation, the ultrasonic pulse transmission method is proposed for measuring gas holdup in gas-liquid two-phase bubbly flows. Two ultrasonic transducers are positioned on opposite sides of a vertical upward pipe with an inner diameter of 20 mm. To obtain the relationship between ultrasonic attenuation and gas holdup, the mean value of the first pulse sequence of ultrasonic signals is first extracted as the measured signal. We used the quick closing valve method to obtain the gas holdup as the set value. Second, the relationship between the gas holdup and measured ultrasonic signals was established. The experiment result shows that the ultrasonic attenuation rate is significantly different at low and high gas holdups, as indicated by the bubble size images with a high-speed camera. We also investigated the ultrasonic field distribution using numerical simulation. The bubble size has an important effect on the ultrasonic attenuation coefficient, which provides a further physical explanation and reference for the experimental phenomena.

Keywords: Gas-liquid Two-phase Bubbly Flow, Gas Holdup, Ultrasonic Measurement Method, High-speed Camera, Sound Field Simulation

INTRODUCTION

Gas-liquid two-phase flow widely exists in industrial production processes, and natural gas is rapidly becoming an increasingly important source of energy [1]. Measurement of the flow parameter is of great significance for optimizing production performance [2]. During the process of dynamic monitoring for an oil well, the gas holdup can be applied to determine the fluid properties, distinguish the region carrying water and measure the gas flow. Furthermore, production profile logging in oil pumping wells typically uses a concentrating flow device to force the mixture fluids in the oil well into a small-diameter measurement channel and to improve the fluid non-uniform distribution. Therefore, it is necessary to develop a method for measuring gas holdup in gas-liquid two-phase bubbly flows in small-diameter pipes.

Due to the complex interphase relative motion and interactions in gas-liquid two-phase flow, bubbly flow exhibits irregularity, randomness and structural instability. Meanwhile, considering the frequent coalescence and breakup between dispersion bubbles, it is extremely difficult to measure the gas holdup. The existing methods for measuring phase holdup include the quick-closing valve (QCV) method, electrical method (conductance or capacitance), optical fiber method, microwave method, scanning imaging method, and ultrasonic method. Among them, the ultrasonic method is a non-contact detection, which means that an ultrasonic sensor is installed on the outside of the pipe to avoid immediate contact with the fluid. This approach makes the fluid encounter little disturbance and is applicable in industrial applications in hostile environments. Based on ultrasonic transmission or reflected signals, the concentration and speed parameters of fluid could be determined. At present, the widely used ultrasonic methods include the transmission technique, reflection technique, Doppler technique [3] and imaging technique [4,5].

The ultrasonic transmission technique is considered one of the most feasible measurement approaches. A pair of ultrasonic transducers is typically installed on opposite sides of the pipe, and the ultrasound generated by the transmitting sensor spreads through the fluid and is finally received by the receiver. The gas distribution in ultrasonic measurement area can be estimated by measuring the ultrasonic amplitude attenuation or propagation velocity [6]. In the actual measurement, the pulsed ultrasound method is typically used to extract the useful information of the fluid such that it avoids the interference of standing waves in continuous ultrasound measurement [7]. The dispersed phase concentration plays an important role in the amplitude of the transmission ultrasound [8], and the ultrasonic attenuation changed with regularity when the gas flow rate increased [9]. Rahiman et al. introduced a mathematical model to explain the influence of a single gas bubble on ultrasound propagation, concluding that the ultrasonic attenuation increased with increases in the bubble diameter [10]. Supardan et al. reported that in a rectangular bubble column, the ultrasonic attenuation has an approximate linear relationship with gas holdup in a certain range [11]. Recently, Murakawa et al. realized the online measurement of the velocity distribution for gas-liquid bubbly flow and slug flow by applying a new multi-wave transducer with the ultrasonic Doppler method [12]. Carvalho et al. proposed an ultrasonic system including one transmitting and three receiving ultrasonic sensors to study the structure of air-water bubbly flows

†To whom correspondence should be addressed.
E-mail: ndjin@tju.edu.cn

[13], and Ito et al. applied an array sensor to obtain visualization images from outside of the pipe without disturbing flows [14]. In addition, numerical methods have been developed for analyzing ultrasonic signals, and Chakraborty et al. used a statistical pattern recognition method called symbolic dynamic filtering to measure the void fraction [15].

Although select progress has been made in the detection of the void fraction of two-phase flows using the ultrasonic method, substantial challenges remain with regard to the relationship between ultrasonic attenuation and gas holdup due to the complex flow structure. In our study, we focused on gas holdup and ultrasonic attenuation in small-diameter pipes and carried out a vertical upward gas-liquid two-phase bubbly flow loop experiment with a round pipe with an inner diameter of 20 mm, which is utilized as the measurement channel in production logging. We measured ultrasonic signals under different gas holdup conditions using the ultrasonic transmission method. Next, we established the relationship between gas holdup and ultrasonic attenuation, and investigated the sound field distribution and theoretical analysis to provide a reasonable physical explanation and reference to the experimental phenomena.

MEASUREMENT PRINCIPLE

1. The Principle of the Ultrasonic Method for Gas Holdup Measurement

The major indicators used to reflect the flow property for ultrasonic measurement are the sound pressure attenuation and ultrasonic transit time [16]. When an ultrasonic wave propagates through the gas-liquid two-phase flow, absorption, scattering and other phenomena occur because of diverse physical properties between the gas and liquid phases, such as density and acoustic impedance; thus, sound energy attenuation occurs. Therefore, the effective flow information in the pipe can be obtained by measuring the ultrasonic energy passing through gas-liquid flow.

The energy attenuation of ultrasound passing through a medium is generally described as follows [17]:

$$dI = -\alpha_0 \cdot L \cdot dL \tag{1}$$

The integral of Eq. (1) can be written as

$$I/I_0 = \exp(-\alpha_0 L) \tag{2}$$

It can also be expressed as

$$-\ln(I/I_0) = \alpha_0 L \tag{3}$$

where I_0 and I are the initial energy at the ultrasonic transmitting terminal and the ultrasonic energy at the propagation distance of L, respectively, and α_0 denotes the ultrasonic energy attenuation coefficient, which is the attenuation degree of ultrasonic energy per unit length.

Because ultrasonic energy is proportional to the square of the sound pressure, Eq. (2) can be expressed as

$$A/A_0 = \exp(-\alpha L) \tag{4}$$

where A_0 and A are the initial sound pressure at the transmitting terminal and the sound pressure at the propagation distance of L, respectively; α represents the attenuation coefficient of the ultrasonic vibration amplitude, which indicates the attenuation degree of ultrasonic vibration amplitude per unit length. As noted above, $\alpha_0 = 2\alpha$. When the pipe is full of water, the sound pressure attenuation is negligible, so that the sound pressures at transmitting and receiving terminals are considered as equality.

To measure the interfacial area of gas bubbles using the ultrasonic technique, Stravs and Stockar [17] and Bensler et al. [18] developed Eq. (4) and proposed the following equation:

$$A/A_0 = \exp\left(-\frac{aL}{8\theta} \cdot \frac{kd_{sm}}{2}\right) \tag{5}$$

where a is the volumetric interfacial area and θ is the scattering coefficient; $k = 2\pi/\lambda$ represents the wave number of the ultrasonic waves, λ is the ultrasound wavelength (m), and d_{sm} is the Sauter mean bubble diameter. To express the amplitude ratio in terms of gas holdup only, the following equation is applied for the volumetric interfacial area a, gas holdup Y_g, and Sauter mean diameter d_{sm}:

$$a = \frac{6Y_g}{d_{sm}} \tag{6}$$

Then, substituting Eq. (6) into Eq. (5), the amplitude ratio is found to be dependent on the gas holdup only and is expressed as

$$A/A_0 = \exp\left(-\frac{3k}{8\theta} \cdot Y_g \cdot L\right) \tag{7}$$

or

$$-\ln(A/A_0) = \left(\frac{3k}{8\theta}\right) Y_g L \tag{8}$$

In addition, Waristo [19] proposed a similar result as follows:

$$-\ln(A/A_0) = X_g Y_g L \tag{9}$$

where X_g depends on the ultrasonic frequency, bubble diameter and physical properties of the fluid. Both Eq. (8) and Eq. (9) show that the attenuation increases with increases in the gas holdup.

2. Factors Influencing Ultrasonic Attenuation

When ultrasound passes through gas-liquid two-phase flow, three main factors result in the ultrasonic energy attenuation [20]: (1) Ultrasonic absorption: Ultrasonic propagation requires a medium, and the propagation process relies on medium molecular vibrations. Then, a portion of the ultrasonic energy is converted into heat. (2) Ultrasonic scattering: Due to the different acoustic impedance between liquid and gas, the ultrasonic scattering phenomenon typically occurs at the gas-liquid interface when the ultrasonic wave spreads in gas-liquid two-phase flow. This leads to ultrasonic energy attenuation in the propagation direction. (3) Ultrasonic diffraction may take place depending on the quantitative relation between the ultrasonic wavelength and bubble diameter.

When the ultrasonic propagation medium is water, the relationship between the ultrasonic frequency f (unit: Hz) and ultrasonic attenuation coefficient a_w (unit: Np/m) is shown as follows [21]:

$$a_w = 25.3 \times 10^{-15} f^2 \tag{10}$$

Because the medium is pure water, ultrasonic scattering and diffraction do not occur. At the moment, the sound pressure atten-

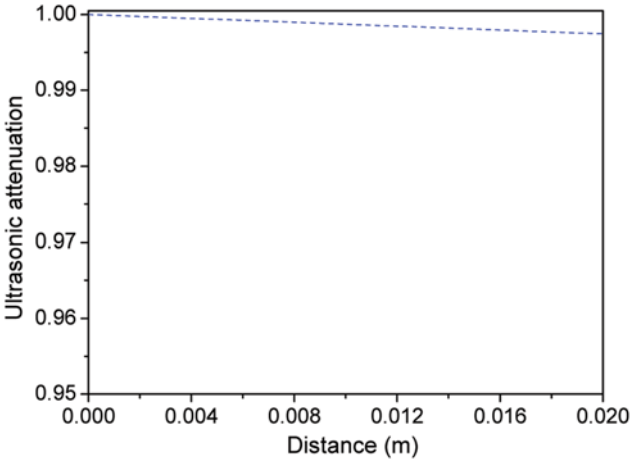

Fig. 1. Theoretical calculation of the ultrasonic attenuation in pure water.

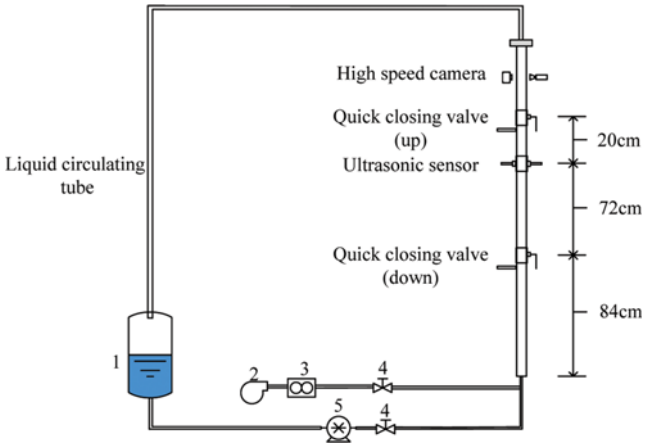

Fig. 2. Schematic of the flow loop facility for the gas-liquid bubbly flow experiment.
1. Water tank
2. Air compressor
3. Float flowmeter
4. Hand ball valve
5. Peristaltic pump

uation coefficient a_w is proportional to the square of the ultrasonic frequency. For an ultrasonic wave with a frequency of 2.25 MHz (used in this article), the sound pressure attenuation coefficient a_w is equal to 0.12808 Np/m and the sound pressure attenuation in terms of the distance calculated by Eq. (3) is shown in Fig. 1.

As shown in Fig. 1, there is only slight ultrasonic sound pressure attenuation caused by water absorption, even when an ultrasonic wave with a 2.25 MHz frequency passes through the pipe from the transmitting sensor to the receiver, A/A_0=0.99744. The sound pressure is only decreased to 99.744% of the original value, and thus, the attenuation caused by the medium of pure water is only 0.256%. This slight attenuation can be ignored. Therefore, the sound pressure at the receiving terminal can be considered equal to the value at the transmitting terminal with the pipe full of water.

When the ultrasound propagates in the inhomogeneous medium, the ultrasonic propagation velocity and medium density differ in different media, and the acoustic impedance Z of the medium is expressed as follows:

$$Z=\rho \cdot c \tag{11}$$

where ρ is the density of the medium (kg/m^3) and c is the sound velocity in the medium (m/s). At the interface of two different media, the ultrasonic reflection coefficient R is

$$R=\left(\frac{Z_2-Z_1}{Z_2+Z_1}\right)^2 \tag{12}$$

where Z_1 and Z_2 are the acoustic impedances of materials 1 and 2, respectively. The acoustic impedance of water and air is 1.494×10^6 and 0.429×10^3 (unit: kg/m^{2}s), respectively, at room temperature, and the distinct difference between them leads 99.89% of the ultrasonic energy to be reflected at the gas-liquid boundary.

The diffraction effect also requires attention. When the ultrasonic wave passes through the bubbly flow with dispersed small bubbles, once the ultrasonic wave length is considerably shorter than the bubble diameter, i.e., $kd_b \gg 1$, the ultrasonic diffraction effect can be ignored [22]. Here, k is ultrasonic wave number and $k=2\pi/\lambda=2\pi f/c$. At this point, the ultrasound effectively encounters an obstacle, e.g., plane, so it cannot bypass the obstacle and diffracts. However, when $k\cdot d_b \ll 1$ or $k\cdot d_b \approx 1$, the diffraction effect cannot be ignored. We discuss this topic below.

EXPERIMENT

1. The Gas-liquid Two-phase Flow Loop Facility and Test

Based on these theories, a gas-liquid two-phase bubbly flow dynamic experiment was carried out with the pulsed ultrasonic transmission measurement method to investigate the relationship between gas holdup and ultrasonic sound pressure in the two-phase flow laboratory of Tianjin University. The schematic of the flow loop facility is shown in Fig. 2. The flow loop facility is composed of a water tank, a peristaltic pump, an air compressor, a float flowmeter, valves and pipes. In this experiment, the inner diameter of the Plexiglas pipe is 20 mm. During the experiment, the water is forced into the bottom of the vertical pipe by adjusting the rotary speed of the peristaltic pump. The air is supplied by the air compressor, and the flow rate is measured by the float flowmeter. Then, water and gas are mixed at the bottom of the pipe, and a mixed fluid develops in the vertical upward pipe. After developing for a given distance (approximately 84 cm), the fluid is fully developed in the test position. The experiment data are measured at this moment. Finally, the fluid flows the water tank, and the gas freely exits the water. The water in the tank is recycled in the experiment.

The test section consists of ultrasonic sensors, two QCVs and a high-speed camera. Transmission type ultrasonic sensors are used to measure the ultrasonic signals under different flow conditions. A high-speed camera is used to shoot the flow structure for different flow conditions. The QCVs are applied to quantify the gas and water holdups. To obtain the gas holdup, the QCVs must be shut off simultaneously. The water holdup and gas holdup are obtained by measuring the water volume fraction between the QCVs. To ensure a high accuracy, the mean value of the gas holdup is determined by trapping the mixture fluids under each flow condition.

The experimental media are air and tap water. During the experiment, both water and air are introduced into the pipe. First,

the gas flow rate is fixed and the water flow rate increases gradually. When the gas and water flow rates remain stable and the mixed fluid fully develops, the response signals of the ultrasonic sensor are collected and the flow structure is recorded by the high-speed camera. After data acquisition, the QCVs are closed simultaneously, as well as the peristaltic pump and air compressor. Thus, the holdup is obtained. When the water flow rate increases to a maximum set value, the gas flow rate is set up to the next flow condition by adjusting the valve opening, and the above steps are repeated. The range of gas phase superficial velocities before mixing with water is from 0 to 0.0737 m/s, and the water phase superficial velocity ranges from 0.5898 to 1.3270 m/s. The experiment includes 60 groups of flow conditions, and the gas holdup varies from 2% to 30%. Due to the limitations of the flow loop facility, it is difficult to mix a small amount of gas with water; thus, the minimal gas holdup is approximately 2%. When the gas holdup is over 30%, the flow pattern gradually changes to a transitional flow pattern, which is a mixture of bubbles and slugs.

2. The Ultrasonic Sensor Measurement System

The ultrasonic sensors are produced by Olympus Corporation (model V323-SU). The diameter and inherent vibration frequency are 6 mm and 2.25 MHz, respectively. The sensors are water immersion transducers and can contact water directly. A schematic of the sensors connected with the pipe is shown in Fig. 3. Two holes are broken on the opposite pipe surface, and the centers of the above holes are in a straight line. The hole size is slightly larger than the transducer diameter; thus, the sensors can be inserted into the hole. The piezoelectric chip top and inner surface of the pipe remain smoothly connected. In the experiment, the rectangular hard plastic was fixed on the pipe to fasten the sensor and prevent leakage.

For the pulsed ultrasonic measurement technique, the ultrasound field is divided into the near- and far-field regions. There are irregular peak values in the near-field region, and the envelope of the acoustic wave in the far-field presents a smooth decay trend. Therefore, the far-field region is typically used for measuring when using ultrasonic transducers. The near-field length N can be calculated by $N=D_0^2/4\lambda$, where D_0 is the sensor diameter. Therefore, if the pipe diameter D is too small, such as when D<N, the measuring region may be located in the near-field region, which results in amplitude measurement error. In contrast, if the

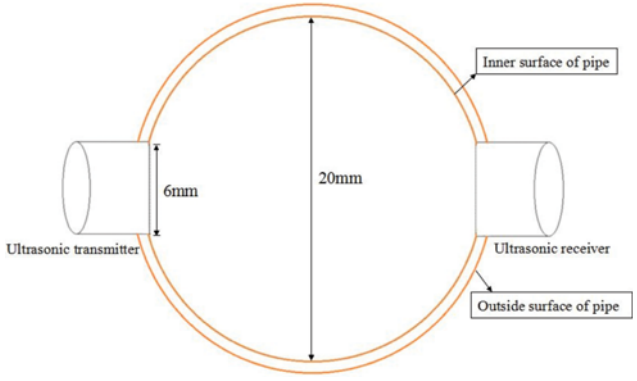

Fig. 3. Schematic of the sensors connected with the pipe.

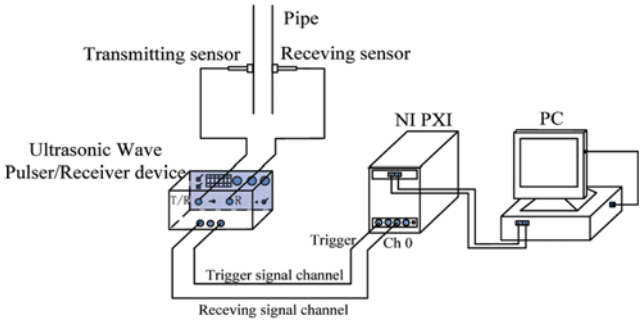

Fig. 4. Schematic of the ultrasonic measurement system.

pipe diameter is too large, such as when D≫N, the ultrasonic amplitude in the measuring region may be too small, which also results in measurement difficulties. Thus, the relative size of the sensor and the pipe diameter should be D>N and ensure that the ultrasonic amplitude in the measuring region can be utilized for monitoring. The sensor and pipe diameter in this research meet the measurement condition.

The ultrasonic measuring system consists of two ultrasonic sensors, one pulser/receiver device, and one piece of data acquisition equipment, as shown in Fig. 4. The sensors are placed at 1,560 mm above the pipe entrance. The pulser/receiver device produces electrical impulses to drive the transducer source and provides the synchronizing signals to the acquisition system. Meanwhile, the pulser/receiver device possesses the function of amplification and filtering to the weak ultrasonic pulse signals from the ultrasonic receiver. The data acquisition system applied is the board card of PXI5112 produced by the National Instrument Company, which has a bandwidth of 100 MHz. The data acquisition program is realized in LABVIEW software, which is used to display and record the real time data.

The pulsed transmission measurement technique using ultrasonic sensors is applied in this experiment. Due to the random structure of the bubbly flow over time and space, there are limitations in measuring a single ultrasonic signal at a certain time. To establish the relationship between ultrasonic signals and ultrasonic sound pressure, the first pulse amplitude sequence of the ultrasonic signals is recorded. According to the amplitude sequence in a period of time, the mean value is calculated as the received ultrasonic signal for this flow condition.

The toggle frequency of the ultrasonic pulses and the sampling were set at 1 kHz and 20 MHz, and after every triggering pulse, the length of the recorded data was 10,000. Each time after every triggering pulse, the maximum value of this trigger can be obtained from the 10,000 recorded points. Furthermore, at each flow condition, 2,000 maximum values with this method will be recorded to construct a maximum sequence. By calculating the average of the maximum sequence, the ultrasonic measurement value can be obtained at this condition.

RESULTS AND DISCUSSION

1. Response of the Ultrasonic Sensor in the Flow Loop Test

The ultrasonic response measured when the pipe is full of water

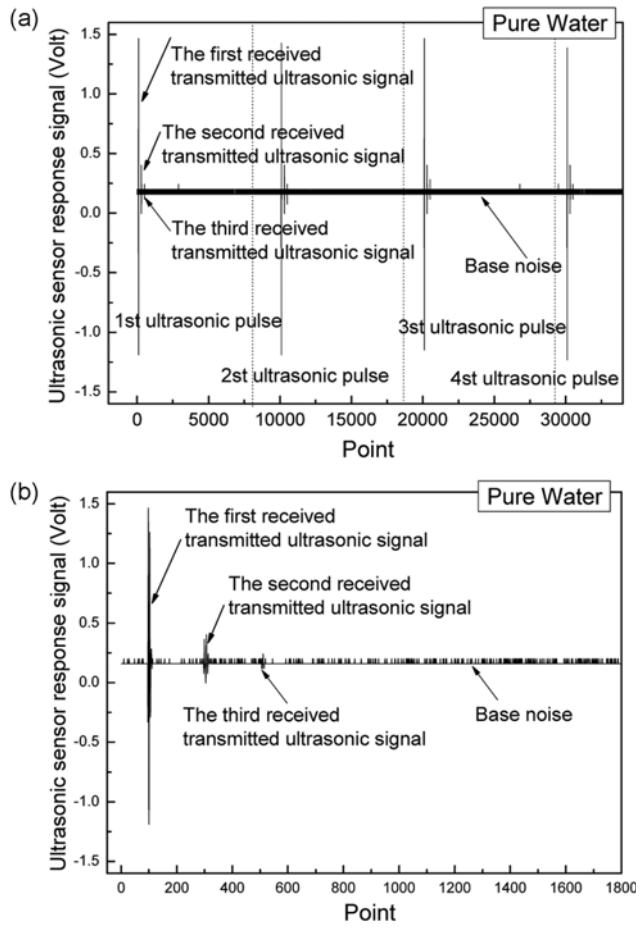

Fig. 5. Collected signals from the ultrasonic receiver (pure water): (a) Signal after four trigger pulses, (b) signal details after a single pulse.

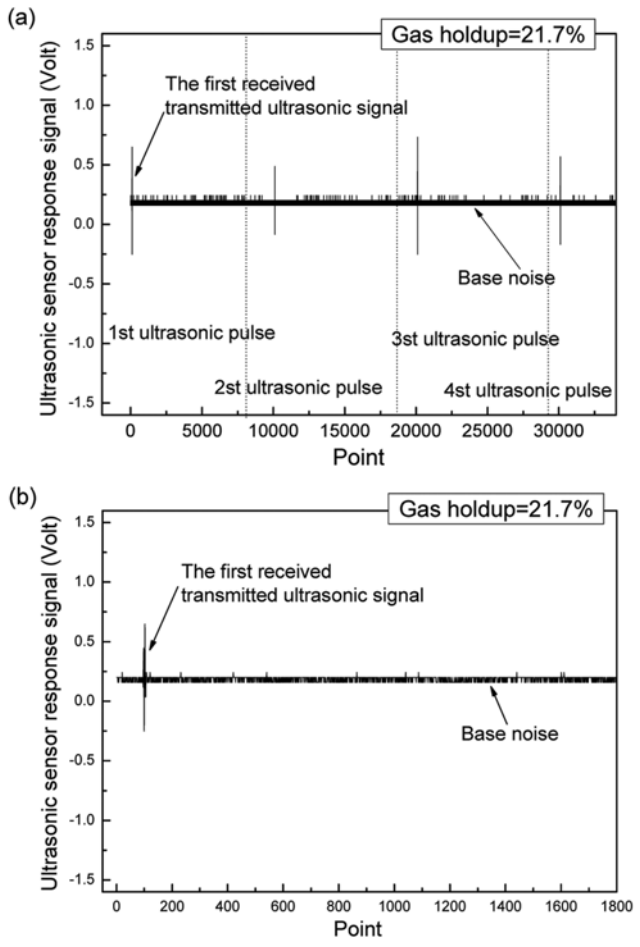

Fig. 6. Signals collected from the ultrasonic receiver (gas holdup= 21.7%): (a) Signal after four trigger pulses, (b) signal details after a single pulse.

is shown in Fig. 5. Fig. 5(a) represents signals after four trigger pulses, and Fig. 5(b) represents the signal details after a single pulse. As the pulsed ultrasonic travels through the fluid, the response signals can be detected by the ultrasonic receiver, and the power of the first received signal is at a high level. After the first pulsed ultrasonic finishes the reflections at the pipe wall, the response is detected by the ultrasonic receiver again. Due to the absorption attenuation at the pipe wall and the scattering attenuation at the dispersed bubbles, the power of the second received signals is at a low level. After further reflection, the power of the received signals becomes gradually lower.

Fig. 6 presents the signals collected from the ultrasonic receiver when the gas holdup is 21.7%. The different peak value for each first received pulse represents that the flow distribution is not constant in the measurement area. Moreover, the minor pulse signals nearly disappear after the first high received transmitted ultrasonic signal, possibly because the second received pulse contains more information relating to the transmission and reflection of ultrasound at the pipe wall, and thus, when the first received pulse is reflected by the pipe wall, the pulse once again is attenuated in the gas-liquid flow, so the second or third received pulse becomes faint.

Based on the acquisition of the ultrasonic sensor responses, the maximum of the recorded data after each triggering pulsed ultrasonic is extracted to construct the first received pulses sequence, called the maximum sequence. The absolute values of the first 2,000 signals received are recorded to construct the maximum sequence. The last measurement result can be determined by calculating the average of the maximum sequence. Several pieces of the maximum sequence in our experiment are shown in Fig. 7. Among them, Fig. 7(a) to Fig. 7(d) show the first 400 received pulses of the maximum sequence when the gas holdups are 4.58%, 14.08%, 20.78% and 28.1%, respectively. The mean values of the maximum sequence from the data acquisition system from Fig. (a) to Fig. (d) are 0.977, 0.731, 0.632 and 0.353, respectively, as marked with the pink line. When the gas holdup increases, the mean value of the ultrasonic maximum sequence gradually decreases. Although the first received signals are not constant, the time-averaging pulsed ultrasonic measurement indicates that the influence of the non-uniformity has been effectively eliminated.

2. Experiment Model of Ultrasonic Attenuation and Gas Holdup

Eq. (8) and Eq. (9) are unified and expressed as

$$-\ln(A/A_0)=\alpha Y_g \tag{13}$$

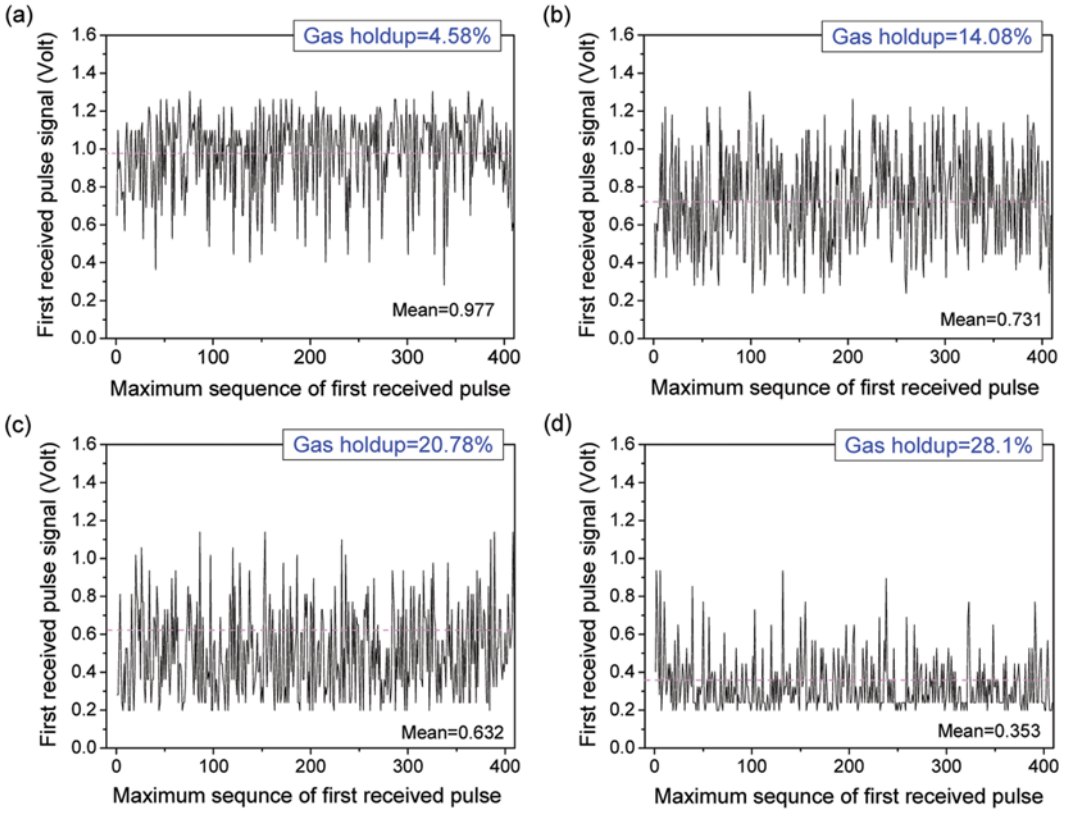

Fig. 7. Maximum sequence of the first received pulse: (a) Gas holdup=4.58%, (b) gas holdup=14.08%, (c) gas holdup=20.78%, (d) gas holdup=28.1%.

In the experiment, the mean value of the first pulse sequence when the pipe is pure water can be considered as A_0 in Eq. (13), and the mean value of the first pulse sequence for gas-liquid two-phase flow can be considered as A; then, the gas holdup can be quantified by the QCVs, and the relationship between ultrasonic attenuation $-\ln(A/A_0)$ and gas holdup Y_g can be established. To determine the sound pressure attenuation coefficient, α, a part of the measured data from the 60 groups of different flow conditions is selected to establish the experimental model. As shown in Fig. 8, the gas holdup Y_g obtained by QCVs is taken as the abscissa, and the ultrasonic attenuation $-\ln(A/A_0)$ is taken as the ordinate. Accordingly, the experimental relationship between the ultrasonic attenuation and gas holdup is determined. The ultrasonic attenuation increases as the gas holdup increases, but the ultrasonic attenuation $-\ln(A/A_0)$ and gas holdup Y_g is not a simple linear relationship. Near the point of Y_g=9.5%, the slope of the experimental curve exhibits a clear change. The measured experimental data were fitted, and the experimental relationship between $-\ln(A/A_0)$ and Y_g is described as follows:

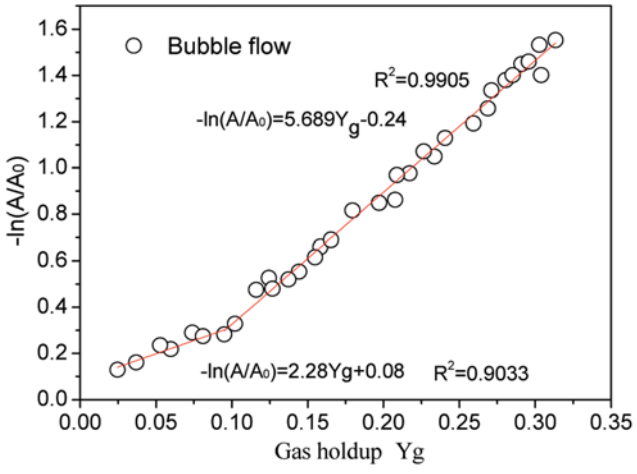

Fig. 8. Relationship between ultrasonic attenuation $-\ln(A/A_0)$ and gas holdup Y_g.

$$-\ln(A/A_0)=\begin{cases}2.28Y_g+0.08 & (2.48\%\le Y_g<9.5\%)\\ 5.689Y_g-0.24 & (9.5\%\le Y_g<30\%)\end{cases} \quad (14)$$

In an earlier study, the results regarding the relationship between ultrasonic attenuation and gas holdup in a rectangular column showed a linear trend [11], which represents that the ultrasonic attenuation coefficient is approximately constant. Fig. 8 illustrates that the increase of the gas holdup causes the rapid attenuation of the ultrasound, but in the two gas holdup ranges, i.e., $2.48\%\le Y_g<9.5\%$ and $9.5\%\le Y_g<30\%$, ultrasonic attenuation and gas holdup present different linear relationships, and the linear correlation coefficients are 0.9033 and 0.9905, respectively. When gas holdup is relatively lower, the slope of the line is smaller, indicating the slow ultrasonic attenuation speed. In contrast, when the gas holdup is relatively higher, the slope of the line is larger, indicating the fast

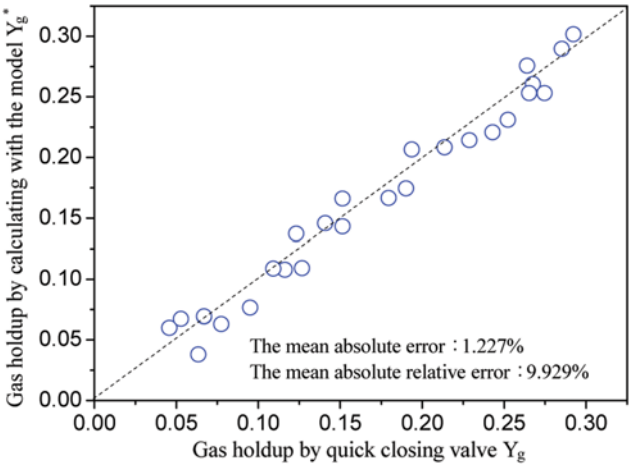

Fig. 9. Comparison of gas holdups between the prediction and QCVs.

ultrasonic attenuation speed. Furthermore, in reference [11], the curve appears to have slight deviations with increasing gas holdup. In this study, the gas holdup range is wider, so one possible reason for the phenomenon is that the attenuation coefficient is different in respective gas holdup ranges, which may be caused by the different bubble diameter. In the following, the possible relationship between the ultrasonic attenuation and bubble size is considered.

Based on the linear fitting, the gas holdup Y_g can be expressed in terms of ultrasonic attenuation as follows:

$$Y_g = \begin{cases} \dfrac{-\ln(A/A_0)-0.08}{2.29} & (0.1297 \le -\ln(A/A_0) < 0.2827) \\ \dfrac{-\ln(A/A_0)+0.24}{5.689} & (0.2827 \le -\ln(A/A_0) < 1.5523) \end{cases} \quad (15)$$

We estimate the errors of gas holdup predicted by Eq. (15) with the experimental data, which are not used in process of modelling Eq. (15). The result is shown in Fig. 9. The mean absolute error of the gas holdup prediction is 1.227%, and the mean absolute relative error is 9.929%. Thus, the experimental data correspond well with the model.

However, the data deviate from the line, and this deviation may originate from two aspects. One measurement error may originate from the data acquisition system. During the experiment, the first received pulse is investigated after each triggered ultrasonic pulse, and the first 2,000 pulses received are recorded to construct a maximum sequence. The ultrasonic measurement value can be obtained by calculating the average of the maximum sequence. Approximately 1.5 minutes is required to record the data at a flow condition. Fig. 5 illustrates that when the pipe is full of water, every first received pulse still has a difference; therefore, the measuring time should be sufficiently long.

Another error that cannot be ignored may originate from the QCVs. In this experiment, two QCVs are used to quantify the gas holdup. To obtain the gas holdup, the QCVs must shut off simultaneously, but in actual operation, it is difficult to shut off the up and down valves synchronously, which may induce another gas holdup error. To reduce the error, the operation of closing the valves is repeated for multiple times to obtain the average gas holdup. Nevertheless, it is still difficult to eliminate experimental errors completely, which causes the deviation in the gas holdup.

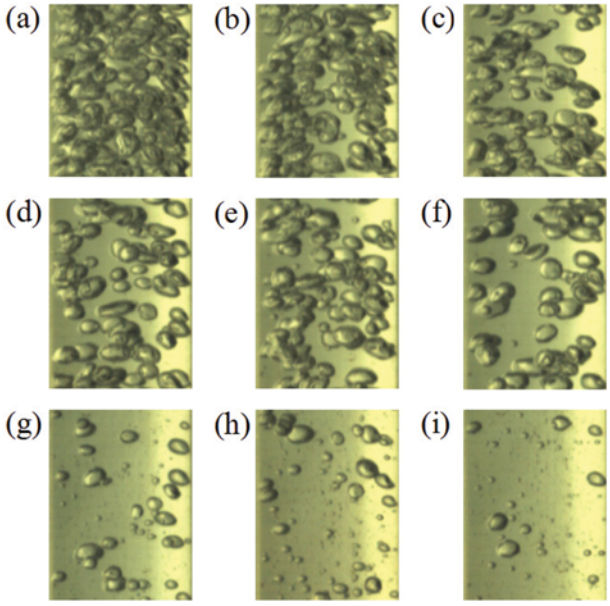

Fig. 10. Instantaneous flow images for different gas holdups by high-speed camera: (a) Y_g=28.5%, (b) Y_g=26.0%, (c) Y_g=24.0%, (d) Y_g=20.0%, (e) Y_g=18.0%, (f) Y_g=13.0%, (g) Y_g=6.0%, (h) Y_g=4.5%, (i) Y_g=2.9%.

3. The Image Information of Flow Structures through a High-speed Camera

A high-speed camera is placed over the ultrasonic sensor outside the pipe. The images are recorded for every flow condition synchronized with the acquisition of the ultrasonic sensor signals. Due to the high fluid velocity, to acquire clear images, the camera resolution is set to 320*240 and the frame rate is 1,200 f/s. In addition, a three-color fluorescent lamp with a flash is applied as the light source, and the color temperature is 6,500 K. The instantaneous flow images for different gas holdups are displayed in Fig. 10.

As shown, for bubbly flow in a small-diameter pipe, the positions of the dispersed bubbles are uneven, as is the bubble size distribution. When the gas holdup is higher (approximately when $Y_g \ge 10\%$), the majority of gas bubbles have relatively large diameters with a few small bubbles scattered between them. When the gas holdup is lower (approximately when $Y_g < 10\%$), the majority of the bubbles are small, and there are some tiny bubbles and a few larger bubbles mixed in them. Comparing the size of the bubbles with the inner diameter of the pipe of 20 mm, the bubble size can be estimated from the images. The result shows that the bubble diameter is distributed from 2 to 3 mm for the higher gas holdup and from 0.8 to 2 mm for the lower gas holdup (mainly small-diameter bubbles). The impact of the bubble diameter on ultrasonic attenuation is discussed below.

4. Simulation of the Different Bubble Sizes and Distribution

For ultrasonic transmission measurement, when a single bubble exists in the pipe, the sound attenuation increases with increases

in the bubble diameter, as illustrated by the computed results through sound field numerical simulation [10,23]. However, for the situation with multiple bubbles in the pipe, the ultrasonic field distribution is also complex and worth exploring. In our previous study, a numerical simulation was used to explain the ultrasound transmission in oil-water flow [24,25]. In this study, a similar approach is used to investigate the ultrasonic field distribution and amplitude loss with respect to the different bubble distribution.

When calculating the distribution characteristic of the ultrasonic measurement field, for the pressure p, an additional first-order term in the time derivative must be introduced to the attenuation model of the sound waves,and the sound field propagation equation is expressed as

$$\frac{1}{\rho_0 c_s^2}\frac{\partial^2 p}{\partial^2 t^2} - d_a\frac{\partial p}{\partial t} + \nabla\cdot\left(-\frac{1}{\rho_0}(\nabla p - q)\right) = Q \tag{16}$$

where ρ_0 refers to the density of the medium, c_s represents the speed of sound, d_a expresses the average bubble size, Q and q are the monopole source and dipole source, respectively. Fluids with bulk viscosities in the same range as air or water exhibit nearly no internal damping over the wavelengths that can be resolved on current computers. Thus, in the numerical computation of the ultrasonic field in this study, we treat the gas and water phases as lossless media, i.e., the damping coefficient is equal to zero. Then, sound wave in a lossless medium is governed by

$$\frac{1}{\rho_0 c_s^2}\frac{\partial^2 p}{\partial^2 t^2} + \nabla\cdot\left(-\frac{1}{\rho_0}(\nabla p - q)\right) = Q \tag{17}$$

Assuming the same harmonic time-dependence for the sources terms, Eq. (17) for acoustic waves reduces to an inhomogeneous Helmholtz equation as follows:

$$\nabla\cdot\left(-\frac{1}{\rho_0}(\nabla p - q)\right) - \frac{\omega^2 p}{\rho_0 c_s^2} = Q \tag{18}$$

where ω represents the angular frequency of the acoustic waves. With the dipole source and monopole source removed, Eq. (18) can be simplified as

$$\nabla\cdot\left(-\frac{1}{\rho_0}(\nabla p)\right) - \frac{\omega^2 p}{\rho_0 c_s^2} = 0 \tag{19}$$

This equation is the continuous-wave equation in the frequency domain. In the experiment, the pulsed-type ultrasonic sensor was used to avoid the negative effect of standing waves. The main advantage of pulsed ultrasound sensors compared with continuous wave ultrasound sensors is avoiding the negative effect of standing waves, which may occur in the acoustic cavity between transducers when the continuous ultrasonic technique is used. If the standing wave phenomenon occurs, incident waves and reflected waves will influence each other, and the ultrasound on the propagation path is weakened and even eliminated, which hinders measurements of the ultrasonic amplitude attenuation. However, the pulsed ultrasound measurement utilizes a pulse sequence to emit the ultrasound sensor, thus preventing standing waves.

The data acquisition system focuses on the first pulsed signal and ignores the other echo signals; thus, the pulsed wave is typically adopted in ultrasonic amplitude measurements. Meanwhile,

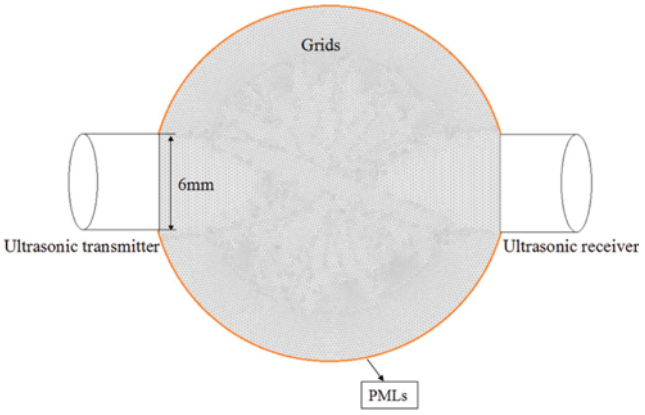

Fig. 11. Meshed finite element model in a pipe with an inner diameter of 20 mm filled with pure water.

to explore the relationship between the phase holdup and received voltage directly, we mainly investigate the first received pulse after each triggered ultrasonic pulse. This means that the reflection signals of ultrasound in the pipe that occur after the first received pulse are ignored.

When investigating the sound field distribution of gas-liquid two-phase bubbly flow under different gas holdup conditions, to construct the finite element model of gas-liquid flow, free meshing is used to divide the models and minimal triangle is chosen as the element type. Meanwhile, the extreme refinement pattern is used in the software. The 2D meshed finite element model of the ultrasonic field is shown in Fig. 11. The transmitting and receiving sensors are placed at the left and right sides of the pipe, respectively, with an inner diameter of 20 mm, and the inner diameter of the ultrasonic transducers is 6 mm.

The 2D model and 3D model are different. In the 3D model, the transducers and bubbles are closer to reality, and the ultrasonic transmission, scattering, and diffraction phenomenon in a 3D space may be simulated precisely. In the 2D plane, the transducers and bubbles can only be represented as rectangles or circular cylinders, respectively, so the ultrasonic simulation result may not be as accurate as that obtained using the 3D method. In the 3D analysis, the ultrasonic attenuation is also influenced by the gas bubble diameter and distribution, as in the 2D analysis. Here, the ultrasonic field is computed numerically to provide insight into the response of the ultrasonic sensor and the influence of the bubble size and distribution on ultrasonic attenuation even though the numerical computation can only indicate trends.

Additionally, the building and meshing of the 3D model of gas-liquid two-phase flow is more difficult, as it is difficult to construct the meshed model because the degrees of freedom (DOFs) in a sufficiently resolved mesh is considerably higher in the 3D model than in the 2D model. The DOFs are difficult to handle in even a 64-bit system model. Moreover, studies on 3D modelling in two-phase flow remain limited, which hinders calculations in the 3D model. Thus, in our study, the 2D model is preferred to simulate the ultrasonic field of the sensor.

In the numerical computation of the ultrasonic field, the boundary condition of the transmitting side (on the left) of the finite ele-

ment model is set as the line source with a frequency of 2.25 MHz, and the perfectly match layers (PMLs) [26] are set as the boundary conditions of the other sides of the model. The PMLs can be treated as an additional domain that absorbs the incident radiation without producing reflections. The reflection at the solid pipe inner wall is real, as shown in Fig. 5. However, in the experiment, to directly explore the relationship between the holdup information and the received voltage, we mainly investigate the first received pulse after each triggered ultrasonic pulse. This means that the reflection of ultrasound at the pipe wall that occurs after the first received pulse can be ignored. Therefore, the PMLs are used to simulate a similar situation in this experiment. However, PMLs cannot be used as the central modelling technique in a time-dependent study. In the COMSOL software, PMLs are only present when using the frequency-domain physics interface, which is why the continuous-wave Eq. (19) is preferred to the impulse

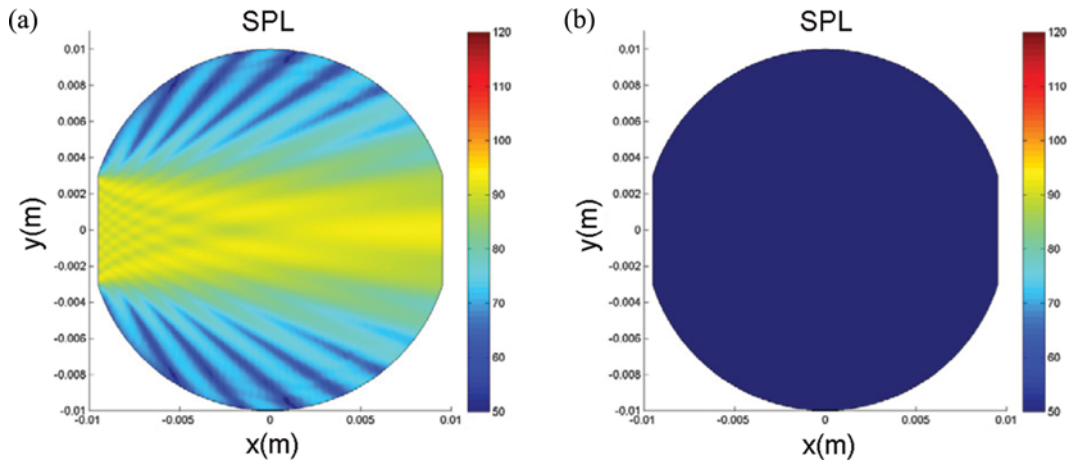

Fig. 12. SPL distribution of the 2D ultrasonic field for a single medium: (a) Pure water, (b) pure gas.

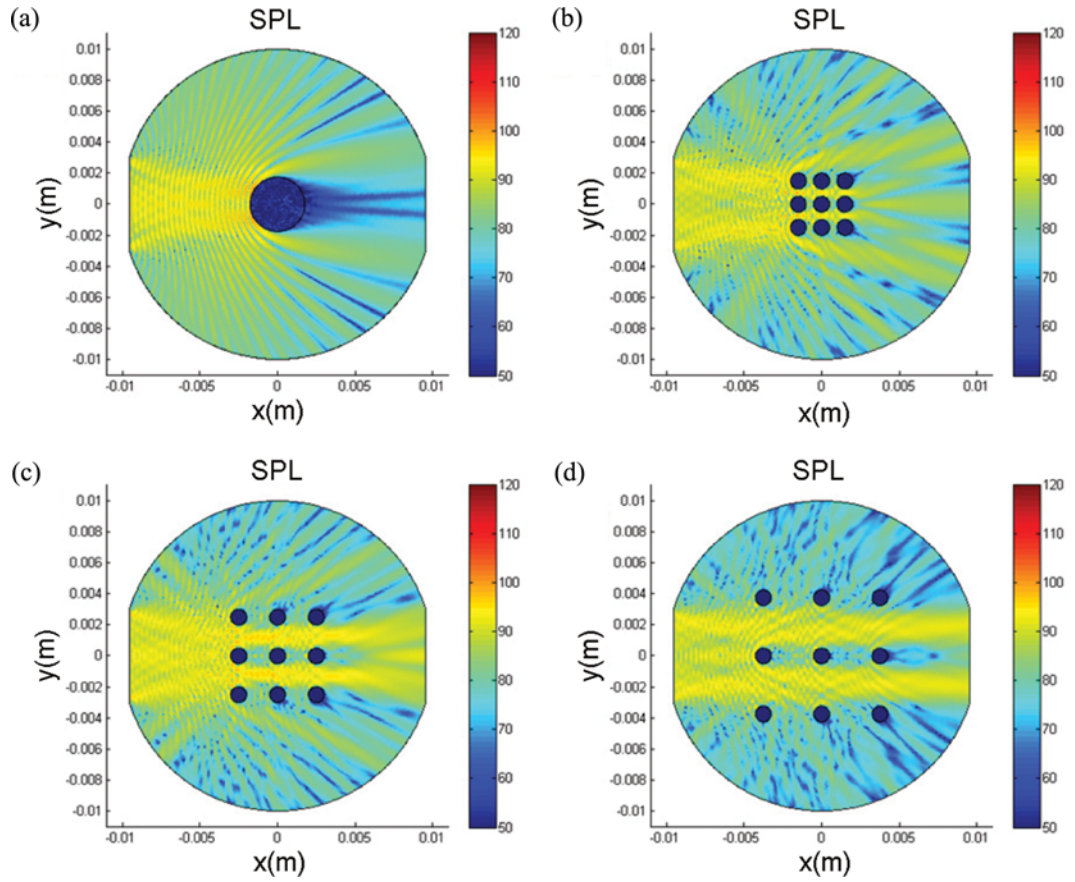

Fig. 13. Numerical simulation of the sound pressure distribution at the same gas holdup of Y_g=2.277%: (a) d=3 mm, (b)-(d) d=1 mm.

response in the finite element calculation.

Figs. 12(a) and (b) show the calculation results for the sound pressure level (SPL) distribution in the ultrasonic field filled with pure water and pure gas, respectively. The brighter area indicates the stronger sound pressure distribution and vice versa. The sound pressure distribution differs greatly due to the different properties of water and gas. When the pipe is full of water, the ultrasound propagates forward in divergent ways from the transmitter, and there is nearly no attenuation at the receiver. When the pipe is full of gas, the sound pressure has a great attenuation and the receiver does not adequately obtain the signal.

As shown in Fig. 12(a), the ultrasonic propagation path includes the main lobe area and side lobe area. The sound pressure in the main lobe area is stronger, and the sound energy is mainly focused on this area. Therefore, the bubbles located in the main lobe area play an important role in sound field distribution. Fig. 13(a) shows the influence of a single bubble with a 3 mm diameter placed at the center of the pipe on sound field distribution. Figs. 13(b)-(d) demonstrate the distributions when nine bubbles with a diameter of 1 mm exist in the main lobe area. The distance between bubbles gradually increases from Figs. 13(b) to (d). The design guarantees the equality of the gas holdups of those situations, and the gas holdup is 2.277%. The ultrasonic amplitude attenuation ratios $(A_0-A)/A_0$ are 16.074%, 15.361%, 7.838% and 1.337% for Figs. 13(a)-(d), respectively, where A_0 is the original signal and A is the receiving one. The amplitude attenuation ratio gradually decreases with increases in the distance between bubbles. The numerical simulation results indicate the following: 1. When bubbles are located in the center of the pipe, the ultrasonic attenuation caused by a single large bubble is greater than that of a few small bubbles for a given gas holdup. 2. For small gas bubbles, the ultrasonic attenuation decreases as the distance between bubbles increases.

In conclusion, the simulation results prove that the different bubble distributions and diameters both affect the ultrasonic attenuation. The ultrasonic attenuation will be weakened when the bubble size becomes smaller or the bubbles disperse farther away. In contrast, the ultrasonic attenuation will be heightened when the bubble size becomes larger, which impedes more ultrasonic energy, resulting in weaker signals being received by the receiving terminal.

5. Theoretical Formula Analysis

For the measuring system with one emission transducer and one receiver, if the transducers are small and placed sufficiently far away, the incident wave is essentially planar and the diffracted energy is negligible [19]. The minimum critical distance for measurement is expressed as $x_0=D_0^2/4\lambda$ [27], where D_0 is the diameter of the transducer and λ is the ultrasonic wavelength. In this experiment, D_0=6 mm, f=2.25 MHz and c=1,497 m/s in water, so the minimal distance is equal to 13.53 mm. Because the inner diameter of the pipe is 20 mm, the ultrasonic sensors meet the experiment conditions. According to this experiment, the largest and smallest bubble diameters are 3 and 0.8 mm, respectively, as calculated from the collected high-speed images. Therefore, k·r is maximized when r is set as 3 mm and minimized when r is equal to 0.8 mm. The corresponding values are 28.331 and 7.555, respectively. Based on the above discussion regarding diffraction phenomenon for bubbly flow, the measurement error caused by diffraction can be ignored when k·r≫1 during this experiment, so the ultrasonic attenuation is mainly caused by scattering. Stravs reported that if the ultrasonic energy attenuation is caused by obstacles, such as gas bubbles, the attenuation coefficient is related to the scattering cross-section. Assuming that the individual scatterers are mutually independent, the attenuation coefficient can be described as follows:

$$\alpha = C_n \int_0^{\infty} s_{n,\,app}(k\cdot r)\cdot \pi \cdot r^2 \cdot f(r)\cdot dr \tag{20}$$

where C_n is the density of bubbles and $\pi\cdot r^2$ represents the projection area of a spherical bubble. f(r) denotes the bubble size distribution and $s_{n,\,app}(k, r)$ is the apparent scattering coefficient, which depends on the scattering coefficient $s_n(k, r)$ and the geometry of the actual experimental apparatus. If the diffraction phenomenon could be ignored in the experiment condition, the apparent scattering coefficient $s_{n,\,app}(k, r)$ is equal to the scattering coefficient, $s_n(k, r)$. Under this condition, a simple fitting relationship of the scattering coefficient was proposed, i.e., $s_{n,\,app}(k, r)=s_n=2+1.442\cdot(k\cdot r)^{-0.57754}$. For a large k·r, the scattering coefficient approaches to 2, and it increases as r increases. Considering that the distribution of bubble size appears to be random and is difficult to describe precisely, f(r) is simulated by mapping out the two-parameter Beta distribution over a range of bubble diameters with varying upper and lower limits, as introduced by Stravs. Here, the upper and lower limits are the largest and smallest bubble sizes, respectively, at a certain flow condition. The two parameters determine the probability distribution type. Žun [28] proposed that the bubbles tend to distribute around the pipe wall when 0.8 mm<d<3.6 mm, so the probability distribution type is similar in this experiment. Thus, f(r) has a similar form in different bubbly flow conditions, indicating that at different gas holdup conditions, the bubble size distribution is nearly the same in the respective bubble size range. Fig. 10 illustrates that as the gas holdup increases, the bubble size r and bubble density C_n increases. Because f(r) has a similar form and $S_{n,\,app}(k, r)$ increases with increasing bubble size, the attenuation coefficient will increase based on Eq. (20). This trend is consistent with the experimental results.

CONCLUSIONS

To discern the relationship between the ultrasonic attenuation and gas holdup for bubbly flow, a flow loop test was conducted to measure the gas holdup with two ultrasonic transducers under 60 groups of bubbly flow conditions. Through the first arrival pulse sequence of receiving ultrasonic signals, the mean value of the sequence was calculated as the measured signal. Meanwhile, the gas holdup obtained by QCVs was used as a set value. Then, the mathematical model was established for predicting gas holdup in gas-liquid bubbly flows. The model for predicting gas holdup was divided into two response lines with different slopes. The research shows that the experimental data correspond well with the established model. In addition, images of the dispersion bubble flow obtained with a high-speed camera illustrate that the diameter of bubble size increases as the gas holdup increases. Furthermore, combining the numerical simulation, the experimental results illus-

trate that increases in the bubble size diameter increases the ultrasonic attenuation coefficient, which can provide a reasonable physical explanation and reference for measuring the gas holdup using the ultrasonic method.

ACKNOWLEDGEMENTS

This study was supported by the National Natural Science Foundation of China (Grant Nos. 51527805, 11572220, and 41174109) and Zhejiang Key Discipline of Instrument Science and Technology (Grant No. JL130106).

NOMENCLATURE

List of Symbols

A : ultrasonic intensity at a transmission distance [V]
A_0 : ultrasonic intensity at transmitting terminal [V]
c : sound speed in the ultrasonic transmission medium [m/s]
d_{sm} : sauter mean bubble diameter [m]
D_0 : transducer diameter [m]
f(r) : bubble size distribution
I : ultrasonic energy at a distance [W]
I_0 : ultrasonic energy at transmitting terminal [W]
k : wave number [m^{-1}]
L : ultrasound transmission path length [m]
$s_{n,app}$: apparent scattering coefficient
s_n : scattering coefficient
X_g : coefficient defined in Eq. (9)
Y_g : gas holdup
Z : acoustic impedance [kg/m^2s]

Greek Letters

α : attenuation coefficient [m^{-1}]
ρ : sound pressure [Pa]
λ : ultrasound wavelength [m]
w : angular frequency of the acoustic wave [rad/s]

REFERENCES

1. J. Lee, M. Yasin, S. Park, I. S. Chang, K. S. Ha, E. Y. Lee, E. Y. Lee, J. Lee and C. Kim, *Korean J. Chem. Eng.*, **32**, 1060 (2015).
2. O. M. H. Rodriguez and R. V. A. Oliemans, *Int. J. Multiphase. Flow*, **32**, 324 (2006).
3. Y. Takeda, *Ultrasonic Doppler velocity profiler for fluid flow*, Springer, Berlin (2012).
4. L. J. Xu and L. A. Xu, *Flow Meas. Instrum.*, **8**, 150 (1998).
5. J. S. Cong, X. M. Wang, D. H. Chen, D. L. Xu, C. X. Che and S. L. Ma, *Chinese J. Geophys.*, **51**, 193 (2008).
6. M. H. F. Rahiman, Z. Zakaria and R. A. Rahim, *Proceedings of the International Conference on Computer and Communication Engineering*, Kuala Lumpur (2008).
7. L. A. Xu, D. Leonard and R. G. Green, *J. Phys. E: Sci. Instrum.*, **18**, 612 (1985).
8. Y. Soong, I. K. Gamwo, A. G. Blackwell, F. W. Harke, R. R. Schehl and M. F. Zarochak, *Ind. Eng. Chem. Res.*, **35**, 1811 (1996).
9. V. Stolojanu and A. Prakash, *Chem. Eng. Sci.*, **52**, 4228 (1997).
10. M. H. F. Rahiman, R. A. Rahim, H. A. Rahim, N. M. N. Ayob, E. J. Mohamad and Z. Zakaria, *Sensor. Actuat. B-Chem.*, **184**, 103 (2013).
11. M. D. Supardan, Y. Masuda, A. Maezawa and S. Uchida, *Chem. Eng. J.*, **130**, 129 (2007).
12. H. Murakawa, H. Kikura and M. Aritomi, *Flow Meas. Instrum.*, **19**, 3 (2008).
13. R. D. M. Carvalho, O. J. Venturini, E. I. Tanahashi, F. Neves Jr. and F. A. Franca, *Exp. Therm. Fluid Sci.*, **33**, 1077 (2009).
14. D. Ito, H. Kikura, M. Aritomi and M. Mori, *J. Phys.: Conference Series*, **147**, 1 (2009).
15. S. Chakraborty, E. Keller, J. Talley, A. Srivastav, A. Ray and S. Kim, *Meas. Sci. Technol.*, **20**, 28 (2009).
16. L. W. Schmerr and S. J. Song, *Ultrasonic nondestructive evaluation systems: models and measurements*, Springer, Berlin (2007).
17. A. A. Stravs and U. Von Stockar, *Chem. Eng. Sci.*, **40**, 1172 (1985).
18. H. P. Bensler, J. M. Delhaye and C. Favreau, *Proceedings of the ANS National Heat Transfer Conference* (1987).
19. Warsito, M. Ohkawa, N. Kawata and S. Uchida, *Chem. Eng. Sci.*, **54**, 4719 (1999).
20. W. R. Hendee and E. R. Ritenour, *Medical imaging physics*, Wiley, New York (2002).
21. H. S. Tapp, A. J. Peyton, E. K. Kemsley and R. H. Wilson, *Sensor. Actuat. B-Chem.*, **92**, 22 (2003).
22. L. J. Xu and L. A. Xu, *IEEE Transactions on Ultrasonics Ferroelectrics and Frequency Control* (1997).
23. M. H. F. Rahiman, H. A. Rahim, N. M. N. Ayob and R. A. Rahim, *Design and development of ultrasonic process tomography*, InTech Open Access Publisher (2012).
24. D. M. Li, L. S. Zhai and N. D. Jin, *Proceedings of the 31st Chinese Control Conference*, Hefei, China (2012).
25. L. S. Zhai, N. D. Jin, Z. K. Gao, Z. Y. Wang and D. M. Li, *Chem. Eng. Sci.*, **94**, 277 (2013).
26. J. P. Berenger, *J. Comput. Phys.*, **114**, 193 (1994).
27. N. Niwa, *Choonpa Keisoku*, Shokodo Press, Tokyo (1982).
28. I. Žun, *Nucl. Eng. Des.*, **118**, 157 (1990).